Journal of Solid State Chemistry **154,** 579–583 (2000)
doi:10.1006/jssc.2000.8897, available online at http://www.idealibrary.com on IDEAL®

Synthesis and Characterization of Homogeneous Germanium-Substituted Tin Oxide by Using Sol–Gel Method

Chika Nozaki,* Kenji Tabata,*,†,[1] and Eiji Suzuki*,†

*Research Institute of Innovative Technology for the Earth (RITE), Kizugawadai, Kizu-cho, Soraku-gun, Kyoto 619-0292, Japan; and
†Graduate School of Materials Science, Nara Institute of Science and Technology (NAIST) Takayama-cho, Ikoma, Nara 630-0101, Japan

Received April 11, 2000; in revised form July 5, 2000; accepted July 28, 2000; published online September 30, 2000

Synthesis of a rutile-type germanium-substituted tin oxide with (110) face was investigated. The characterization was performed by XRD, SEM, TEM, EDX, IR, XPS, and BET surface area measurements. When the percentage of germanium contained was less than 10 wt%, the homogeneous rutile-type germanium-substituted tin oxide was obtained. The obtained oxide had a homogeneously germanium-substituted (110) face. © 2000 Academic Press

INTRODUCTION

Rutile tin oxide, SnO_2, has received wide attention with much work related to the use of the material in for example gas sensing (1–6) and oxidation catalysis (7–13). Especially, the lowest energy (110) face has been focused because it has been revealed to have unique surface properties such as the presence of several surface oxygen species (such as O^-, O_2^{2-}, and O_2^-) (14–18) and the capability of oxygen desorption at relatively low temperature (15, 19, 20). Therefore, the synthesis of partly substituted tin oxide with more effective properties for gas sensing and more highly reactive catalysis is quite important.

In general, the utilization of molecular oxygen for oxidation reactions is a rewarding goal since it has the highest content of active oxygen and forms no by-products. In addition, the lowering of reaction temperature is a key requirement for oxidation reactions because the high temperatures and pressures lead to successive oxidation to CO_x. Therefore, the presence of active oxygen species (O^-) is quite important for oxidation reactions because it allows oxidation reactions to proceed at low temperatures. However, the activity was still low because only a small amount of active oxygen species was formed (18).

[1]To whom correspondence should be addressed. E-mail: kenjt@rite.or.jp. Fax: 81-774-75-2318.

To improve the surface properties of the (110) face, we tried to synthesize a rutile-type germanium-substituted tin oxide. It was expected that the properties of surface oxygen species could change by replacing tin atoms with germanium atoms; i.e., with the same IVB group metal, its ionic crystal radius is smaller than that of tin, and its electronegativity is higher than that of tin. The important requirements for synthesis of germanium-substituted tin oxide are as follows: (1) rutile-type structure is maintained, (2) germanium atoms are completely solubilized in SnO_2 structure, and (3) germanium atoms are substituted in the surface of SnO_2.

The synthesis of germanium-containing tin oxide with perovskite structure, for example, $SnGeO_3$, has been reported (21). However, the synthesis of germanium-substituted tin oxide with a (110) face of rutile structure has never been reported.

In this paper, we reported the synthesis and characterization of homogeneous germanium-substituted tin oxide with a (110) face by using a sol–gel method.

EXPERIMENTAL

The reagents used were commercially obtained and used without further purification. The synthesis of germanium-substituted tin oxide (Ge = 6.7 wt%, abbreviated as **I**) was carried out as follows: $Sn(OC_2H_5)_4$ (0.5 g) and $Ge(OC_2H_5)_4$ (0.05 g) were mixed and dissolved in ethanol (10 mL) under Ar atmosphere. To the clear solution, acetophenone (0.33 g) was added. After 1 h of stirring, the solution was stabilized in the air. After about 2 weeks, a wet gel was formed. The solid was placed in an oven (423 K) for 24 h to form xerogel. The hard xerogel was then ground to a fine powder. The fine powder of **I** was calcined at 423–1273 K under the atmosphere for 10 h. The obtained powder was white. The BET surface areas of **I** calcined at 973 and 1273 K were 78.2 and 3.64 m^2/g, respectively.

Powder X-ray diffraction (XRD) patterns were recorded with a powder X-ray diffractometer (Rigaku, Inc.) by using

0022-4596/00 $35.00

monochromatic Cu$K\alpha$ radiation. The cell constants of the samples were determined from high angle reflections. XRD data were collected by step scanning over an angular range $5^\circ \leq 2\theta \leq 90^\circ$ in increments of 0.01° (2θ).

Infrared spectra of samples in the KBr pellets were recorded with a magna-IR spectrometer 550 (Nicolet, Inc.). X-ray photoemission spectra (XPS) were recorded with a Shimadzu ESCA-KM spectrometer equipped with a concentric hemispherical analyzer. Transmission electron micrograph (TEM) and scanning electron micrograph (SEM) analyses were carried out with an S-5000 (Hitachi, Inc.) and a HF-2000 (Hitachi, Inc.), respectively. EDX analyses were carried out with EMAX-5770 (Horiba, Inc.) and Sigma (Kevex, Inc.). BET surface areas were measured on AUTOSORB-1 (Quanta Chrome Co.).

RESULTS AND DISCUSSION

Figure 1 shows the XRD patterns of **I** calcined at 423, 773, 973, and 1273 K, respectively. The XRD pattern of **I** in Fig. 1d had mainly three lines at $2\theta\,(^\circ) = 26.730$, 34.060, and 51.980 with relative intensities of 100, 89, and 67, respectively. These main three lines were assigned to the (110), (101), and (211) faces, respectively, and as the characteristics of tetragonal rutile structure (12, 22). The lattice constants were $a = 4.7126$ Å and $c = 3.1697$ Å. No peaks of other impurities were observed. The structure of **I** changed from amorphous state to fine crystal as the temperature of calcination was raised from 423 K up to 1273 K.

Figure 2 showed the plot of the values of lattice constants *versus* the percentage of germanium contained for the rutile-type oxides. These plots showed that the values of the lattice constants, a and c, decreased linearly with the increase in percentage of germanium contained in the range of 0.0–6.7 wt%. However, the plot deviated from the solid line at 15.0 and 42.0 wt%. The TEM–EDX analyses of germanium-containing tin oxides (15.0 and 42.0 wt%) revealed that the percentage of germanium contained homogeneously in the crystal was less than 10 wt%. In addition, at 60 wt%, the germanium-containing tin oxide had a hexagonal structure. These facts suggested that the germanium atoms were completely solubilized in the rutile SnO_2 structure in the range of 0–10 wt% under our synthetic conditions.

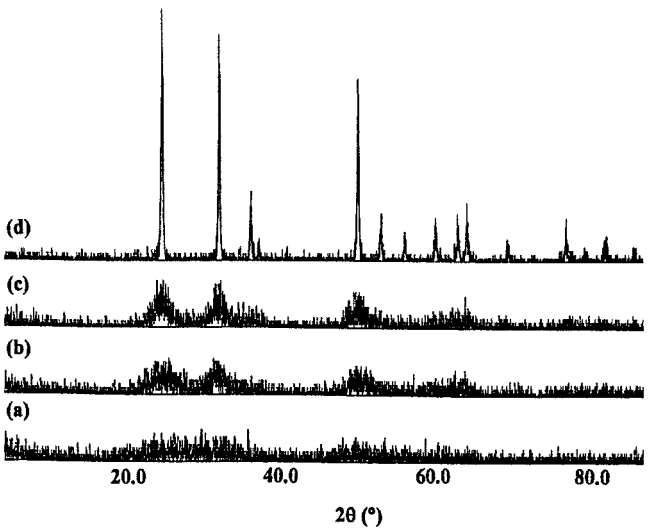

FIG. 1. XRD patterns of **I**. Temperatures of calcination were (a) 423 K, (b) 773 K, (c) 973 K, and (d) 1273 K.

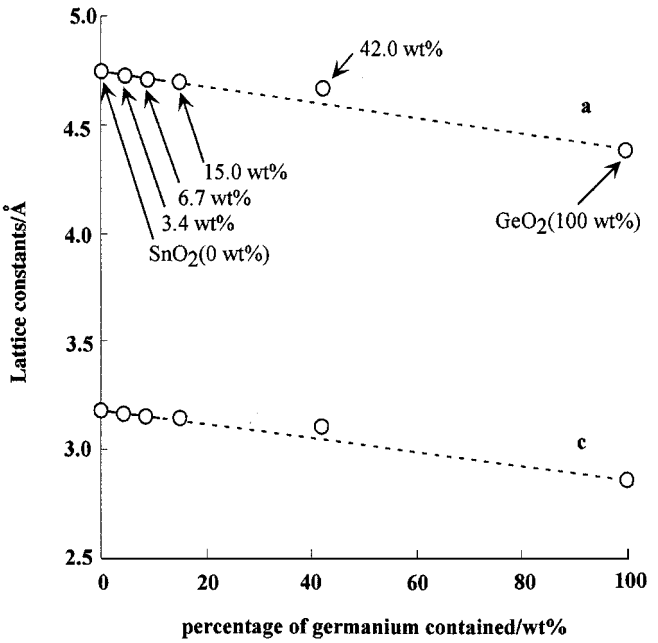

FIG. 2. Plots of the values of lattice constants *versus* the percentage of germanium contained for the rutile-type oxides. The lattice constants of rutile-type GeO_2 were referenced in JCPDS card.

Figure 3 shows the SEM micrographs. **I** calcined at 973 and 1273 K consisted of particles with sizes of 10–20 and 10–150 nm, respectively. The average particle sizes of **I** calcined at 973 and 1273 K were 15.0 and 65.3 nm, respectively. The particle size distribution of **I** calcined at 973 and 1273 K is also shown in Fig. 3. It is clear that the particle size distribution of **I** calcined at 973 K is small and the size distribution is narrow; in contrast, that of **I** calcined at 1273 K is bigger and the size distribution is wide. The SEM–EDX analysis of **I** calcined at 973 K revealed Sn was 89.98 ± 0.88 wt% and Ge was 10.02 ± 0.88 wt%. The observed composition of **I** calcined at 1273 K was Sn, 90.13 ± 0.74 wt%, and Ge, 9.87 ± 0.74 wt%. The theoretical composition of **I** was Sn, 93.26 wt%, and Ge, 6.74 wt%. Thus, these values were approximately consistent with the theoretical composition. The observed composition was almost the same in different places of the sample. This result showed that **I** was a homogeneous oxide. The SEM images also showed that the structure of **I** changed from amorphous state to fine crystal as the

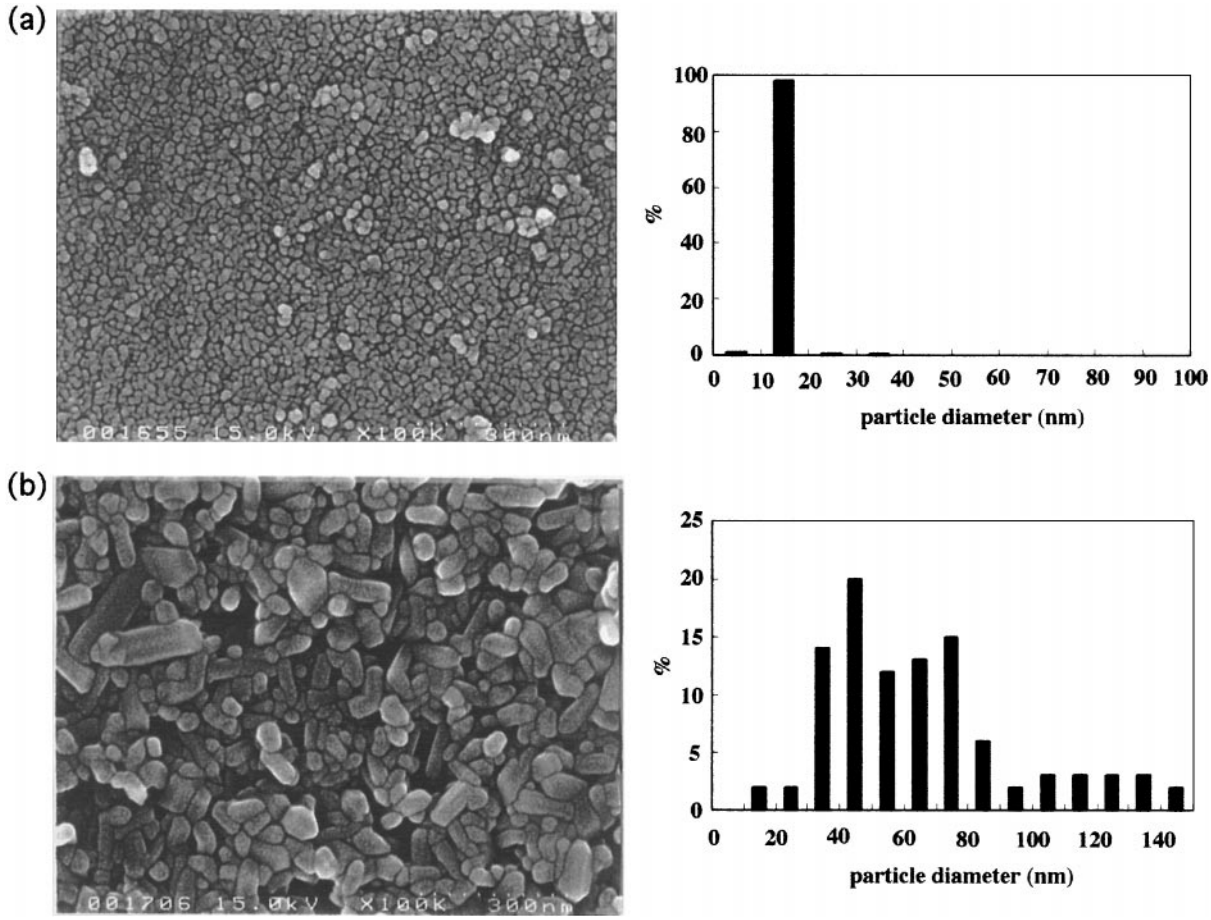

FIG. 3. Scanning electron micrographs and particle size distribution of **I** calcined (a) at 973 K and (b) at 1273 K.

temperature of calcination was raised from 423 K up to 1273 K.

The electron diffraction patterns of **I** showed that both particles calcined at 973 and 1273 K were fine crystals. The TEM–EDX analysis of crystals of **I** calcined at 973 K revealed that Sn was 91.78 ± 2.54 wt% and Ge was 8.22 ± 0.75 wt%. The observed composition of **I** calcined at 1273 K was Sn, 92.83 ± 1.28 wt%, and Ge, 7.17 ± 0.35 wt%. These values of **I** calcined at 973 and 1273 K were approximately consistent with the theoretical composition and agree with those observed by SEM–EDX analyses. The percentage of crystal lattice in the TEM images also showed that the structure of **I** changed from amorphous state to fine crystal as the temperature of calcination was raised from 423 K up to 1273 K. These results of SEM and TEM measurements suggested that the Sn/Ge ratio of **I** did not change with the increase in calcination temperature. The calcination temperatures mainly contribute to the development of a crystal of **I**. Therefore, the obtained oxide calcined at 1273 K was the best germanium-substituted SnO_2 crystal with (110) face of rutile structure.

Infrared spectra of the sample showed that the typical C–H vibrational bands observed in the regions of 3800–2700 cm^{-1} and 1450–1375 cm^{-1} (23) disappeared after calcination. It is clear that the organic species included

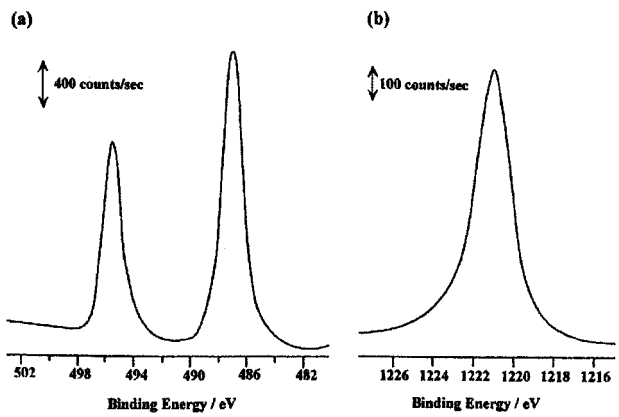

FIG. 4. XPS spectra of **I** calcined at 1273 K: (a) Sn3*d* level and (b) Ge2*p* level.

in starting materials, such as alkoxides, acetophenone, and ethanol, are removed.

Figure 4 showed the XPS spectra of Sn3*d* and Ge2*p* levels of **I** calcined at 1273 K. In Fig. 4a, the binding energy (E_B) was calibrated with the Sn^{4+} ($3d_{5/2}$) peak as 486.7 eV (24–26). In Fig. 4b, the peak of Ge2$p_{3/2}$ level was observed at $E_B = 1221.3$ eV. The atomic sensitivity factors of Sn3$d_{5/2}$ and Ge2$p_{3/2}$ were 4.3 and 6.1, respectively (27). Thus, the atomic ratio of [Sn]/[Ge] of **I** was about 9.1. This value was appropriately in good agreement with the theoretical ratio. This result suggests that the Sn/Ge ratio of the surface of **I** calcined at 1273 K is equal to that of the bulk.

Figure 5 showed the XPS spectra of Sn3*d* and O1*s* levels of SnO_2 and **I** calcined at 1273 K. The E_B was also calibrated with the Sn^{4+} ($3d_{5/2}$) peak at 486.7 eV. It has been reported that the E_B differences between the binding energies of metal and oxygen (ΔE_B) showed the electron states of metal–oxygen bonds in metal oxides (28). In our case, the ΔE_B (O1s − Sn3$d_{5/2}$) of SnO_2 was calculated to be 43.9 eV. This value was in good agreement with the value in Ref. (29).

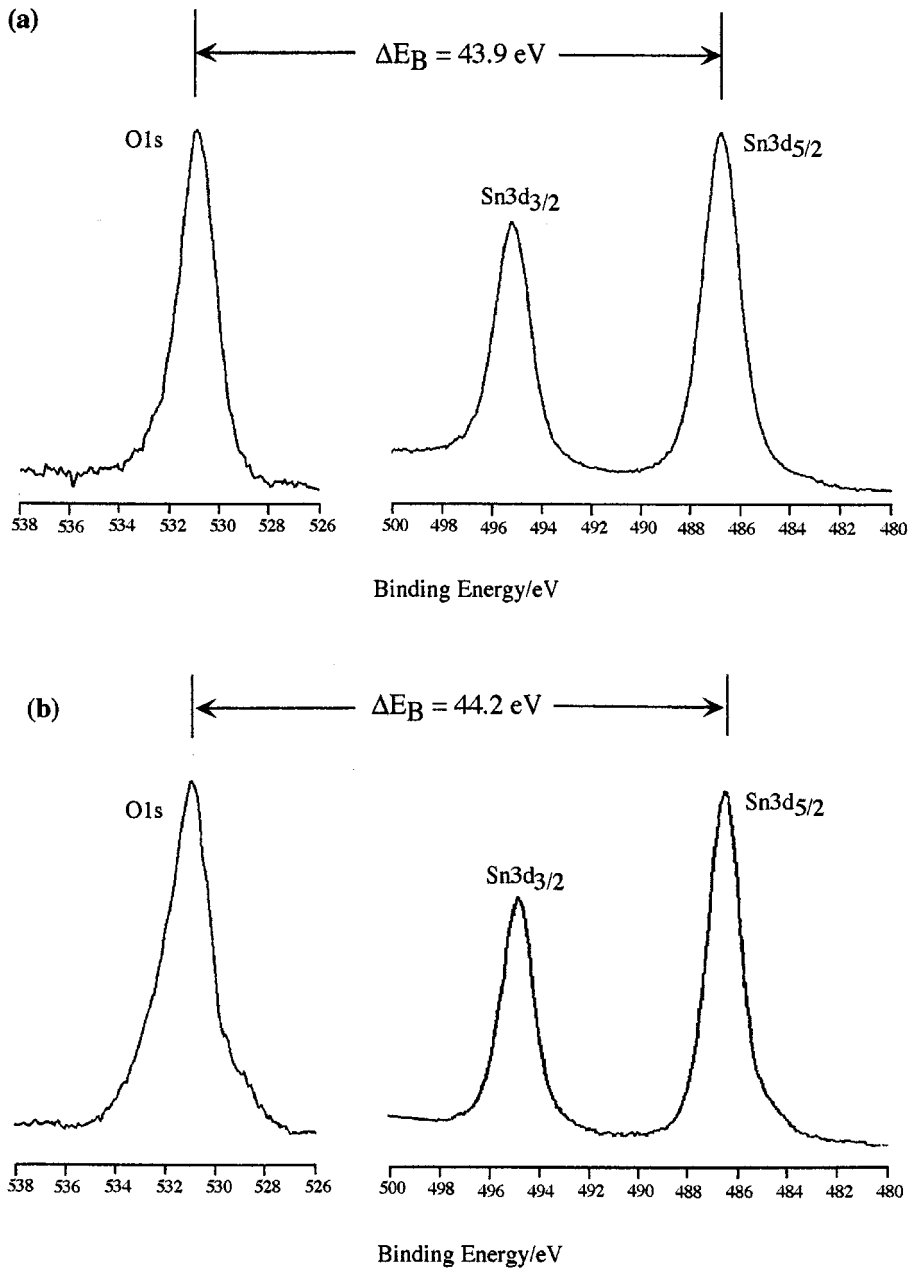

FIG. 5. XPS spectra of Sn3*d* and O1*s* levels of (a) SnO_2 and (b) **I** calcined at 1273 K.

TABLE 1
Chracterization Results of I Calcined at 1273 K

Characterization methods	Results
XRD	Lattice constants: $a = 4.7126$ Å, $c = 3.1697$ Å,
SEM	Average particle size: 65.3 nm
SEM–EDX	Sn, 90.13 ± 0.74 wt%; Ge, 9.87 ± 0.74 wt%
TEM–EDX	Sn, 92.83 ± 1.28 wt%; Ge, 7.17 ± 0.35wt%
BET surface area	3.64 m^2/g
XPS	Sn/Ge = 9.1
XPS	ΔE_B (O1s − Sn3$d_{5/2}$) = 44.2 eV

The ΔE_B (O1s − Sn3$d_{5/2}$) of **I** was calculated to be 44.2 eV. Thus, the difference between ΔE_B values of SnO_2 and **I** was 0.3 eV. This value suggested that the electron state of metal–oxygen was changed by replacing tin atoms with germanium atoms in the SnO_2 structure. Therefore, this result supported that the germanium atoms were substituted in the rutile-type SnO_2 structure.

The characterization results of **I** calcined at 1273 K are summarized in Table 1. These results showed that (1) the obtained oxide, **I**, had a rutile-type structure, (2) germanium atoms were homogeneously solubilized in SnO_2 structure, (3) **I** was a crystal with an average size of 65.3 nm, (4) germanium atoms substituted were present homogeneously in the surface of **I**, and (5) the Sn/Ge ratio of surface of **I** was equal to that of bulk.

CONCLUSION

In conclusion, the present results demonstrate that the synthesis of homogeneously germanium-containing tin oxide with the (110) face of rutile structure is possible in the range of 0–10 wt%.

ACKOWLEDGMENTS

This study was supported by the New Energy and Industrial Technology Development Organization (NEDO, Japan). We also acknowledge Mrs. Y. Ichikawa (RITE) for SEM and TEM measurements.

REFERENCES

1. G. Sberveglieri (Ed.), "Gas Sensors," Kluwer Academic, Dordrecht, 1992.
2. D. E. Williams and K. F. E. Pratt, *J. Chem. Soc. Faraday Trans.* **94,** 3493 (1998).
3. D. E. Williams and K. F. E. Pratt, *J. Chem. Soc. Faraday Trans.* **91,** 1961 (1995).
4. D. E. Williams and K. F. E. Pratt, *J. Chem. Soc. Faraday Trans.* **92,** 4497 (1996).
5. D. E. Williams, G. S. Henshaw, K. F. E. Pratt, and R. Peat, *J. Chem. Soc. Faraday Trans.* **91,** 4299 (1995).
6. Y. Nagasawa, K. Tabata, and H. Ohnishi, *Appl. Surf. Sci.* **121/122,** 327 (1997).
7. F. J. Berry, *Adv. Catal.* **30,** 97 (1981).
8. R. Pearce and W. R. Patterson, "Catalysis and Chemical Processes," Leonard Hill, 1981.
9. I. Brown and W. R. Patterson, *J. Chem. Soc. Faraday Trans. I* **79,** 1431 (1983).
10. J. McAtcer, *J. Chem. Soc. Faraday Trans. I* **75,** 2768 (1979).
11. D. R. Pyke, R. Reid, and R. J. D. Tilley, *J. Chem. Soc. Faraday Trans. I* **76,** 1174 (1980).
12. L. T. Weng, N. Spitaels, B. Yasse, J. Ladrière, P. Ruiz, and B. Delmon, *J. Catal.* **132,** 319 (1991).
13. V. A. Gercher, D. F. Cox, and J. M. Themlin, *Surf. Sci.* **306,** 279 (1994).
14. P. Meriaudeu, C. Naccache, and A. J. Tench, *J. Catal.* **21,** 208 (1971).
15. G. L. Shen, R. Casanova, and G. Thornton, *Vacuum* **43,** 1129 (1992).
16. S.-C. Chang, *J. Vac. Sci. Technol.* **17,** 366 (1980).
17. J. H. C. van Hooff and J. F. van Helden, *J. Catal.* **8,** 199 (1967).
18. Y. Nagasawa, T. Choso, T. Karasuda, S. Shimomura, F. Ouyang, K. Tabata, and Y. Yamaguchi, *Surf. Sci.* **433–435,** 226 (1999).
19. M. Iwamoto, Y. Yoda, N. Yamazoe, and T. Seilyama, *J. Phys. Chem.* **82,** 2504 (1978).
20. D. F. Cox, T. B. Fryberger, and S. Semancik, *Surf. Sci.* **224,** 121 (1989).
21. J. Silver, E. A. D. White, and J. D. Donaldson, *J. Mater. Sci.* **12,** 827 (1997).
22. W. K. Choi, J. S. Cho, J. Cho, S. C. Choi, H.-J. Jung, and S. K. Koh, *J. Korean Phys. Soc.* **31**, 369 (1997).
23. R. M. Silverstein, G. C. Bassler, and T. C. Morrill, "Spectroscopic Identification of Organic Compounds," 4th ed. John Wiley & Son, New York, 1981.
24. C. L. Lau and G. K. Wertheim, *J. Vac. Sci. Technol.* **15,** 622 (1978).
25. R. Sanjinès, C. Coluzza, D. Rosenfeld, F. Gozzo, Ph. Alenéras, F. Lévy, and G. Margaritondo, *J. Appl. Phys.* **73,** 3997 (1993).
26. L. Kövér, Z. Koyács, R. Sanjinés, G. Moretti, I. Cserny, G. Margaritondo, J. Pálinkás, and H. Adachi, *Surf. Interface Anal.* **23,** 461 (1995).
27. D. Briggs and M. P. Seah, "Practical Surface Analysis," 2nd ed. John Wiley & Sons, New York, 1990.
28. T. L. Barr, "Modern ESCA," CRC Press, Boca Raton, FL, 1994.
29. S.-K. Song, W.-K. Choi, J.-S. Cho, H.-J. Jung, D. Choi, J.-Y. Lee, H.-K. Baik, and S.-K. Hoh, *J. Appl. Phys.* **36,** 2281 (1997).